

Electron transport and energy degradation in the ionosphere: evaluation of the numerical solution, comparison with laboratory experiments and auroral observations

D. Lummerzheim¹, J. Lilensten²

¹ Geophysical Institute, University of Alaska, Fairbanks, AK 99775-7320, USA

² CEPHAG ENSIEG, BP 46, F-38402 St Martin d'Hères Cedex, France

Received: 16 July 1993/Revised: 14 April 1994/Accepted: 20 April 1994

Abstract. Auroral electron transport calculations are a critical part of auroral models. We evaluate a numerical solution to the transport and energy degradation problem. The numerical solution is verified by reproducing simplified problems to which analytic solutions exist, internal self-consistency tests, comparison with laboratory experiments of electron beams penetrating a collision chamber, and by comparison with auroral observations, particularly the emission ratio of the N_2 second positive to N_2^+ first negative emissions. Our numerical solutions agree with range measurements in collision chambers. The calculated N_2P to N_2^+1N emission ratio is independent of the spectral characteristics of the incident electrons, and agrees with the value observed in aurora. Using different sets of energy loss cross sections and different functions to describe the energy distribution of secondary electrons that emerge from ionization collisions, we discuss the uncertainties of the solutions to the electron transport equation resulting from the uncertainties of these input parameters.

1 Introduction

The primary cause of the aurora is precipitation of energetic electrons. These electrons are guided by the geomagnetic field, and being accelerated to a kinetic energy of several keV well above the thermosphere, penetrate into the atmosphere of increasing neutral density. They lose their energy through collisions with the ambient gas, leaving neutrals and ions in vibrationally and electronically excited states and giving rise to the luminosity of the aurora. The energy that they release is converted to radiation and heat, and it provides a source of energy to feed a plethora of neutral and ionic chemical reactions in the ionosphere. In order to construct models of the aurora, its

luminosity, and its effects on the thermosphere it is necessary to understand and model the transport of electrons into the atmosphere.

Many different approaches have been taken to achieve knowledge of the electron distribution of the auroral precipitation throughout the thermosphere. The rigorous solution of a transport and energy degradation equation can be avoided by a range calculation (Rees, 1963; Vallance Jones, 1974). For this approach an energy deposition function which is obtained from laboratory experiments of electrons penetrating a collision chamber is scaled to the real atmospheric densities (Grün, 1957; Barrett and Hays, 1976). This method yields some optical emission rates and ionization rates in reasonable agreement with many auroral observations. Range calculations cannot give information about the angular redistribution of precipitating electrons due to elastic scattering nor do they include discrete energy loss in inelastic scattering events. This limits the application of range calculations to high energy particles. For more detailed studies of auroral electron transport, numerical methods are employed to solve a linear Boltzmann transport equation. Berger *et al.* (1970) adopted a Monte Carlo code and presented results on the spreading of an auroral arc perpendicular to the ambient geomagnetic field. The photoelectron transport and thermalization was solved by Mantas (1974) with an iteration method. Two-stream solutions of the transport equations were obtained by Nagy and Banks (1970), Banks and Nagy (1970), Banks *et al.* (1974), Stamnes (1980, 1981), Richards and Torr (1985), Link *et al.* (1988) and others. Jasperse (1976) applied a diffusion approximation to solve the photoelectron transport equation, and presented an analytic approach to the auroral electron transport problem (Jasperse and Strickland, 1981). Cicerone *et al.* (1973) compared three different numerical solutions to the electron transport equation for the photoelectron case, including diffusion, two-stream, and Monte Carlo codes. Strickland *et al.* (1976) presented a solution to the electron transport equation that resolved the pitch angle distribution of the penetrating stream of electrons. This method of solution was based on solving

the transport equation with a predictor corrector scheme, and reducing the energy degradation and scattering to an eigenvalue problem by extrapolation on a numerical grid in energy and pitch angle. Later the numerical scheme was further refined and the transport equation was solved as an eigenvalue problem (Strickland *et al.*, 1983, 1989). Stamnes (1980, 1981), Link (1982), Porter *et al.* (1987), and Lummerzheim *et al.* (1989) solve the electron transport equation by separating the energy degradation from the transport and scattering equation, albeit using different numerical methods. Porter *et al.* (1987) solve the transport and scattering equation with an iterative method, while Lummerzheim *et al.* (1989) have adopted a discrete ordinate method. Most recently, Link (1992) has outlined a method that is derived from the Feautrier method, and Solomon (1993) has developed a Monte Carlo solution.

A comprehensive auroral model must combine an acceleration mechanism for electrons and protons above the ionosphere, a particle transport calculation, and an ionospheric model that can determine the response of the ionosphere to the precipitation. Because of the importance of electron transport calculations to auroral models, we evaluate the numerical solution of the electron transport and energy degradation equation. The particle precipitation does not only cause the auroral emissions but provides a major energy source that modifies the local ionosphere. The effects of precipitating particles are observed by ground based or rocket or satellite borne optical instruments, by incoherent scatter radars, and by in situ measurements of ionospheric parameters. Using the results from electron transport calculations, Strickland *et al.* (1983, 1989) relate UV and EUV auroral brightnesses to characteristics of the electron precipitation and composition of the neutral atmosphere. Lummerzheim *et al.* (1990) deduce the neutral composition from the brightness of visible auroral emissions. Liliensten *et al.* (1990) have studied the auroral heating of the ionosphere by combining data from incoherent scatter radar with electron transport calculations.

Simultaneous satellite observations of precipitating electrons and emissions from the $N_2^+ 1N$ (first negative) band suggest that for most aurorae the brightness of the $N_2^+ 1N$ band is a good measure of the energy flux of the precipitation, independent of the spectral shape of the electron distribution (Kastings and Hays, 1977). This conclusion is also supported by the various electron transport calculations. Other emissions have observable surface brightnesses that are not independent of the spectral shape or characteristic energy of the precipitating electrons. The brightness of UV emissions is strongly controlled by the absorption of UV light in the atmosphere between the emission and the observer. If such an emission is normalized to a precipitation with unity energy flux, its surface brightness gives an indication of the altitude of the emission and thus the mean energy of the incident electron intensity (Strickland *et al.*, 1983). In particular measurements of brightness ratios from a satellite can be interpreted in this way (Rees *et al.*, 1988; Ishimoto *et al.*, 1988; Germany *et al.*, 1990; Lummerzheim *et al.*, 1991). The OI doublet at 6300 Å derives its sensitivity to the mean energy of the precipitation from the

altitude dependence of the mixing ratios, the temperature of the neutral atmosphere, and the altitude dependence of collisional de-excitation of the long-lived parent state of the OI(6300) doublet. The red to blue ratio (OI(6300)/ $N_2^+ 1N$) has long been used as an indicator for the mean energy of precipitating electrons in aurora (Rees and Luckey, 1974; Vallance Jones *et al.*, 1987; Christensen *et al.*, 1987). Based on the electron transport calculation by Lummerzheim (1987), Rees and Lummerzheim (1989) suggested that the ratio of $N_2 2P$ (second positive) brightness to $N_2^+ 1N$ brightness might also show a dependence on mean energy. However, observational evidence by Gattinger *et al.* (1991) shows this brightness ratio to be independent of the spectral hardness of the incident electron intensity. Model calculations by Strickland *et al.* (1989), Richards and Torr (1990), and Solomon (1993) also find this ratio to be independent of the characteristic energy of the electron precipitation. Recent calculations with a new transport code based on the Lummerzheim (1987) code are in agreement with the other models and the measurements by Gattinger *et al.* (1991). We present this new transport calculation in this paper and compare the results to observations in the auroral atmosphere and to laboratory measurements.

2 The transport equation for electrons

2.1 The transport equation

A one-dimensional transport equation for the guiding centers of precipitating electrons can be derived from the Boltzmann equation. This equation describes the electron intensity I (in units of $eV^{-1} cm^{-2} s^{-1} ster^{-1}$) as a function of scattering depth τ , energy E , and pitch angle μ (μ is the cosine pitch angle; for the southern hemisphere we reverse the sign of μ so that the terms downward and upward refer to negative and positive values of μ independent of the hemisphere) as follows.

$$\begin{aligned} \frac{\mu}{\sin \alpha} \frac{\partial I(\tau, E, \mu)}{\partial \tau} - n_e \frac{\partial(LI)}{\partial E} = & -I(\tau, E, \mu) \\ & + \frac{\omega(\tau, E)}{2} \int_{-1}^1 p(E, \mu' \rightarrow \mu) I(\tau, E, \mu') d\mu' \\ & + Q(\tau, E, \mu; I). \end{aligned} \quad (1)$$

The angle between the geomagnetic field and the horizontal is α . This angle allows a slanted geomagnetic field to be taken into account, but this formulation is restricted to homogeneous fields, i.e. we neglect the magnetic mirror force. Min *et al.* (1993) have shown that it is possible to solve this equation with a mirror force and a small field aligned electric field. The energy loss to the ambient electrons with density n_e is described by the loss function $L(E)$ ($eV cm^2$) (Swartz *et al.*, 1971); $\omega(\tau, E)$ is the scattering albedo which is the ratio of the elastic collision frequency to the total collision frequency; $p(E, \mu' \rightarrow \mu)$ is the phase function for elastic scattering which gives the probability of an incident electron at energy E with pitch angle μ' to scatter to the pitch angle μ ; and $Q(\tau, E, \mu; I)$ combines all

internal sources including locally produced photoelectrons, energy degraded electrons from inelastic collisions at higher energy levels, and secondary electrons from ionizing collisions. The energy degradation source at a given energy E is determined from the intensities at higher energy levels E' as follows.

$$Q(\tau, E, \mu; I) = Q_{local}(\tau, E, \mu) + \sum_j n_j(z) \int_E^{\infty} \sigma_j(E' \rightarrow E) \times \frac{1}{2} \int_{-1}^1 p_j(E', \mu' \rightarrow \mu) I(\tau, E', \mu') d\mu' dE'. \quad (2)$$

The local sources such as photoelectron production are combined in Q_{local} . The sum extends over all species and all states of each species with density n_j , cross section σ_j and phase function for inelastic collisions p_j . Scattering in inelastic collisions is predominantly in the forward direction, and the angular redistribution in inelastic collisions is negligible compared to elastic collisions. In the following we thus assume that the phase function p_j can be approximated by a Dirac δ -function in the forward direction for inelastic collisions, and that secondary electrons from ionization collisions are distributed isotropically. Laboratory cross section measurements by Opal *et al.* (1972) show that the angular distribution of secondary electrons has an energy dependent peak approximately 60° from the direction of the incident electron. We have used our transport code in numerical experiments to evaluate the importance of using the correct angular distribution of secondaries. Using phase functions for two extreme cases, secondaries generated isotropically and in the forward direction, we found that the angular redistribution function (double differential cross section) for secondary electrons has no influence on the altitude profiles of heating rates, energy deposition rates, and emission rates. The angular distribution of the low energy electrons is dominated by elastic scattering, while the production of secondaries dominates the energy distribution. It suffices to use single differential (in energy) cross sections for ionization collisions.

The transport equation is expressed as a function of the scattering depth rather than altitude. The scattering depth τ is related to the altitude z by

$$d\tau = - \sum_j \sigma_j^{tot}(E) n_j(z) dz, \quad (3)$$

where σ_j^{tot} is the sum of the elastic, excitation, dissociation, and ionization cross sections and n_j is the neutral density of the j -th atmospheric species.

2.2 Energy degradation

Solving this transport equation (Eq. 1) consists of two distinct and separable tasks: the determination of the energy degradation source term, and the penetration into the atmosphere and angular redistribution. The transport equation is solved subject to boundary conditions in altitude and energy. At some high altitude, the downward

electron intensity is specified as a function of energy and pitch angle, and at some low altitude we specify an upward electron intensity. The lower boundary is selected such that the scattering depth is so large that transport becomes negligible and zero upward intensity can be assumed. For the boundaries in energy we assume that above the upper limit of the chosen energy interval no precipitation occurs and the degradation source vanishes. The lower limit is given by the crossover of the streaming electron population and the ambient thermal electron population. This boundary is open and electrons crossing it contribute to the heating of the ambient electron gas.

Starting at the highest energy level, the transport equation is solved for penetration and angular scattering at that energy. This provides the intensity for Eq. (2) and the degradation source term for the next lower energy can be determined. This process is repeated until the solution for all energies is found. Numerical errors that occur during the penetration of energy degradation calculation are compounded and propagate through the energy grid. This requires that the energy degradation calculation must produce minimal round-off errors. For the energy range that is dominated by secondary electrons from ionization collision at much higher energy, the compounded numerical error has minimal effect, since only a few degradations contribute to the source. Likewise, if a source such as photoelectrons or secondary electrons resulting from precipitating protons is included, the relative contribution to the source of the compounded numerical error is reduced.

Numerical difficulties arise in the degradation calculation when an electron of several keV energy loses a few eV in a collision. There have been several methods suggested to resolve such losses on a numerical energy grid. The simplest approach is the use of a fine mesh of many grid points (Link, 1992), but the aforementioned compounding error and the required large number of grid points limit this approach to fairly small primary electron energies. This method finds applications in photoelectron and soft precipitation calculations. An energy degradation scheme based on pseudoparticles which are spread out over a range of energies is employed by Porter *et al.* (1987). Strickland *et al.* (1989) use a two-dimensional extrapolation scheme in energy and pitch angle to determine the degradation and angular scattering simultaneously. Their suggested extrapolation is based on combined sums of powers of μ and powers of $\log E$. With this method Strickland *et al.* (1989) get satisfactory results with less than 100 energy grid points to cover the energy interval from thermal energy to several tens of keV. In our treatment of the transport equation the energy degradation is treated separately from the penetration and angular scattering. We have adopted the energy degradation scheme proposed by Swartz (1985), in which the intensity and cross sections are approximated by step functions. This method requires a dense energy grid for adequate representation of the intensity. The procedure requires defining effective cross sections that accommodate the energy losses in collisions on a given numerical energy grid. The energy grid is given by energy cells of increasing size. We find that approximately 200 grid cells suffice for transport calculations for auroral electrons.

The accuracy of the numerical treatment of the energy degradation calculation can be evaluated independently of the transport equation. Consider an altitude region of very large scattering depth, $d\tau \rightarrow \infty$, assume that only one neutral species is present which has only one loss process with a given cross section. Then $\partial I(\tau, E, \mu)/\partial \tau = 0$ and $\omega = 0$ and Eq. (1) may be written as

$$\sigma(E)I(E) = \int_T^{\infty} \sigma(E' \rightarrow E)I(E')dE', \quad (4)$$

where $\sigma(E)$ is a loss cross section with a discrete energy loss of magnitude T , giving

$$\sigma(E' \rightarrow E) = \sigma(E')\delta(E - (E' - T)), \quad (5)$$

with the Dirac δ -function. Equation (4) describes energy degradation without transport and scattering. If one specifies a simple analytic form for the loss cross section, Eq. (4) can be solved analytically. We have solved the same equation with our numerical energy degradation scheme for a number of energy grids with varying resolution, and found good agreement with the analytic solutions.

A requirement that must be fulfilled by the differential cross section for non-ionizing collisions in general is given by

$$\int_0^E \sigma(E \rightarrow E')dE' = \sigma(E). \quad (6)$$

This is simply the requirement that the source of degraded electrons from energy E to any other energy E' must equal the loss of all electrons from energy E . If we restrict the ionizing collisions to single ionizations and exactly one secondary electron is produced in an ionization, then the requirement of Eq. (6) also holds for ionizing collisions

$$\int_0^E \sigma^{sec}(E \rightarrow E')dE' = \sigma^{ion}(E), \quad (7)$$

where $\sigma^{sec}(E \rightarrow E')$ is the cross sections for an incident electron of energy E to produce a secondary electron at energy E' . Both of these conditions serve as a test for the discretized differential cross sections. Both conditions are satisfied by our code for realistic cross sections and energy distribution functions to the accuracy available with single precision arithmetic.

2.3 Scattering and penetration

It is also desirable to test the penetration and scattering calculation that we adopt for the solution of the electron transport equation. For a fixed energy, and a given source term Q in Eq. (1), the equation is formally equivalent to a radiative transfer equation. There are many well proven numerical methods available for radiative transfer calculations. Photon scattering often involves extremely sophisticated phase functions to resolve the detailed angular behavior of scattered light. Wiscombe (1977) has devised a method to include phase functions with a single large forward peak into a discrete ordinate solver. This makes it particularly well suited for electron transport, since scattering at high energies is predominantly in the forward

direction. The theoretical basis for a numerical solution of a multiple scattering transport problem, using the discrete ordinate method, has been reviewed by Stamnes (1986). This numerically stable algorithm led to the development of a radiative transfer code, DISORT, by Stamnes *et al.* (1988). This code is suitable for a variety of applications and is used in atmospheric radiation problems, cloud physics, and particle transport. Stamnes and Conklin (1984) describe details of the numerical method, and evaluate the stability and accuracy of the code and how they depend on the number of streams and atmospheric layers. They compare reflectivity and transmissivity as calculated by DISORT with results using other proven numerical methods. Their comparisons include cases with isotropic and anisotropic scattering, finite layers and semi-infinite atmospheres. They conclude that the DISORT code achieves an accuracy of better than 1% for their test cases, if 8 or more streams are used. Stamnes *et al.* (1991) have also evaluated and verified the DISORT code by applying it to a number of problems including transport and thermalization of a gas in a host medium consisting of a different gas. They give examples of cases with external sources, imbedded sources, and consider the thermal escape problem. Lie-Svendsen *et al.* (1992) present a study of the helium escape from the Earth's atmosphere, using the DISORT code to solve the scattering and transport equation.

We adopt the DISORT code for the electron transport calculations with a modification to allow anisotropic internal sources as suggested by Stamnes *et al.* (1991). Running DISORT in combination with the energy degradation source for electron transport, we studied the behavior of our results when changing the computational grids. By doubling the number of layers we find that for most auroral problems we get no further changes in our results if we increase the grid beyond 100 atmospheric layers. For isotropic incident spectra, we find that 8-stream calculations suffice to describe the angular scattering, provided that the strong forward peak of the phase function at high energies is treated with the δ -M method of Wiscombe (1977). The scattered fluxes at any specific energy change by less than 3% between a four-stream and an eight-stream calculation, and by less than 0.5% between an eight-stream and a 16-stream calculation. Energy integrated fluxes and height integrated emission rates change by less than 0.4% between a four-stream and eight-stream case, and by less than 10^{-4} between an eight-stream and a 16-stream case. In order to resolve anisotropic spectra a higher number of angular streams might be desirable in specific cases.

3 Input to the transport calculation

3.1 Cross sections

Precipitating electrons and photoelectrons interact with the neutral atmosphere through elastic and inelastic collisions. These cause the electrons to scatter in angle and degrade in energy. For the solution of the transport equation we need to know cross sections for energy loss and

scattering, phase functions describing the angular distribution of scattered electrons, and energy degradation functions giving the energy distribution of degraded primary and secondary electrons. In order to calculate auroral emission rates and brightnesses we also need emission cross sections and absorption cross sections for the emitted photon.

Cross section sets for auroral electron transport have been assembled by several authors. Green and Stolarski (1972) presented analytic approximations of cross sections for electron impact on the three major neutral species in the thermosphere, Jackman *et al.* (1977) have presented a collection of cross sections, and Wadzinski and Jasperse (1982) published a collection of about 150 cross sections for electron impact on neutrals. Lummerzheim (1987) used a set of integrated cross sections that were compiled from published laboratory measurements and that is being updated when new measurements become available. Similar cross section sets are maintained by Strickland *et al.* (1989) and Solomon (1993). We have used different combinations of cross section sets, and have found that the electron transport results depend on the choice of the particular set of cross sections. Stamnes and Rees (1983) investigated the effect of different cross section sets on photoelectron transport calculations. Their recommendation forms the basis of the cross section set used by Lummerzheim (1987), hereafter referred to as set 1. This

set has evolved from Pritchford and Phelps (1982) and is modified by Lummerzheim (1987). Lilensten *et al.* (1990) used this and the set by Oran and Strickland (1978) (hereafter set 2), and found large differences in the heating rate computed from precipitating electrons. The total inelastic cross sections from these sets are shown in Fig. 1 together with the cross sections from Solomon (1993). We have updated both sets and use identical N_2 and O_2 ionization cross sections for our comparisons in both sets. These are taken from Rapp and Englander-Golden (1965) and Borst and Zipf (1970). The $N_2(C^3\Pi)$ excitation cross section in the set used by Stamnes and Rees (1983) is larger than the values in set 2, and we have reduced this cross section in set 1 to bring it into agreement with set 2 and with the measurements by Cartwright *et al.* (1977). Remaining differences in the two sets stem from uncertainties of cross section measurements as presented in the literature, and from the selection of excited states that are included in the sets. The latter is particularly apparent in the large difference in the O_2 cross sections above about 50 eV. Set 1 contains cross sections that are averages for excitation into combinations of several unidentified states and that are defined by their associated mean energy loss (4.5 eV, 6.0 eV, 8.4 eV, and 9.7 eV) (Stamnes and Rees, 1983), while set 2 has cross sections that are identified by state: $A^3\Sigma_u$ (4.7 eV loss), $B^3\Sigma_u$ (8.5 eV loss), two Rydberg states (14 eV and 18.7 eV loss), and an unidentified

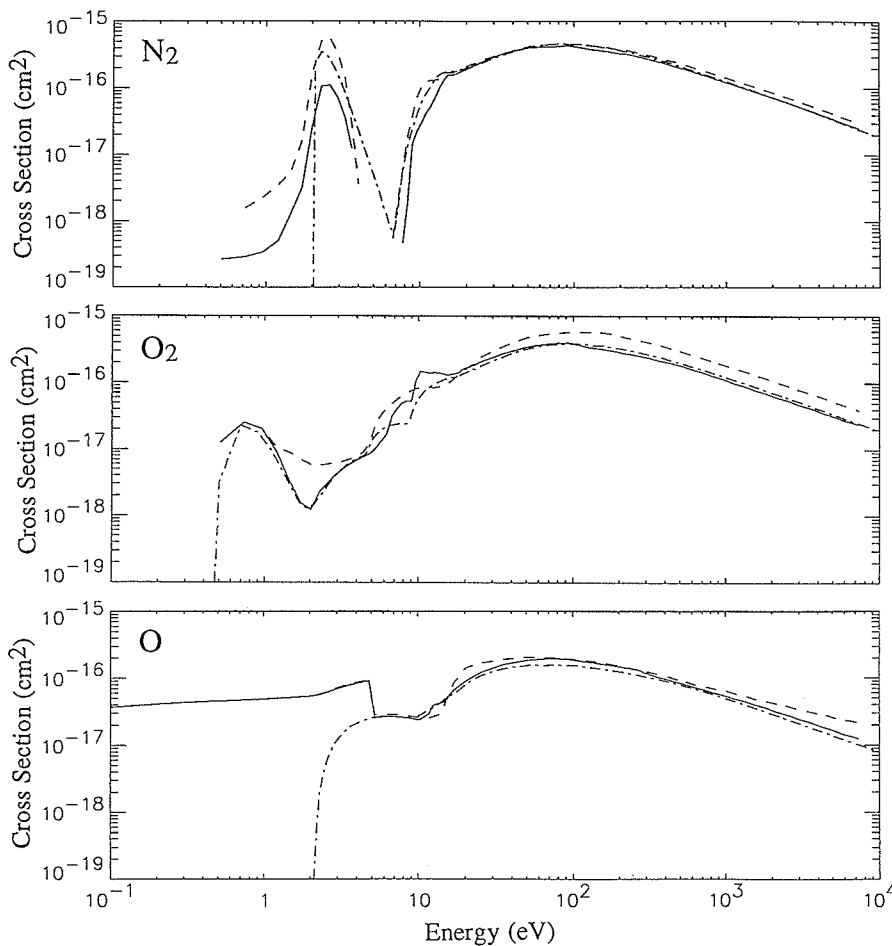


Fig. 1. Total inelastic cross sections for N_2 , O_2 , and O from three different compilations of cross sections. Set 1 (Lummerzheim, 1987) is shown as a *solid line*, set 2 (Oran and Strickland, 1978) as a *dashed line*. Also shown is the total cross section from Solomon (1993) as a *dash-dot line*

average process with 9.9 eV energy loss. Set 2 tends to have larger cross sections and larger energy losses for the individual excited states. This results in less penetration into the atmosphere and slightly higher emission altitudes in auroral electron transport calculations.

3.2 Phase function for elastic scattering

As indicated in Eq. (1) we separate the angular differential scattering cross section into a product of the cross section and the normalized phase function that describes the pitch angle redistribution, $p(E, \mu' \rightarrow \mu)$. Measurements of the angular differential cross sections for collisions of electrons with atmospheric constituents are available, and have been parameterized by Porter and Jump (1978). This parameterization is given by

$$p(\cos \Theta) = \frac{1}{N} \left[\frac{1}{(1 + 2\gamma - \cos \Theta)^2} + \frac{\beta}{(1 + 2\delta + \cos \Theta)^2} \right], \quad (8)$$

where Θ is the total scattering angle, and the tabulated values for β , γ , and δ fit the phase function to laboratory measurements in the energy range from 2 eV to 1 keV. Tables for these parameters are given in Porter and Jump (1978) and Porter *et al.* (1987). The normalization N is given by

$$N = \frac{1}{4} \left[\frac{1}{\gamma(1 + \gamma)} + \beta \frac{1}{\delta(1 + \delta)} \right]. \quad (9)$$

For energies above 1 keV we set $\beta = 0$ so that Eq. (8) becomes identical to the screened Rutherford phase function, where γ is the screening parameter. This parameterization is widely used for auroral electron transport (e.g. Lummerzheim *et al.* 1989; Link, 1992; Solomon, 1993). Porter *et al.* (1987) discuss the sensitivity of transport calculation results to changes in this parameterization.

3.3 Differential cross sections for energy degradation and secondary electron production

The energy loss experienced by an incident electron in a non-ionizing inelastic collision is assumed to equal the excitation energy of the target. The mass ratio between electrons and the neutral collision targets in the atmosphere is so large that energy transfer from the electron into kinetic energy of the target can be neglected. The minimum energy loss of the electron is the excitation threshold of the excited state of the target. Excitation of vibrational levels of the excited target molecule consumes an additional amount of energy. In particular the excitation of the $N_2(a^1\Pi_g)$ state, which gives rise to the LBH emission, has been studied in detail by Ajello and Shemansky (1985). Their laboratory measurements are in agreement with aurora and dayglow observations and indicate that the cross section for excitation of the vibrational level $v' = 3$ is more than three times larger than for the level $v' = 0$. The energy loss for excitation of the $v' = 3$ level is 9.16 eV, compared to 8.55 eV for the $v' = 0$ level.

The energy needed for vibrational excitation may be accounted for by using an energy loss that is higher than the threshold of a given collision process. We investigate the sensitivity of the transport calculation to small changes of the energy loss by arbitrarily increasing the energy loss by 5% and 10% from the threshold energy for all states.

In ionizing collisions the energy of the incident electron is distributed between the excitation and ionization energy of the target and the emerging two electrons, which we identify as the secondary and primary electron according to their energy. The energy loss of the incident electron is thus the sum of the excitation and ionization energy and the kinetic energy of the secondary electron. We write the differential cross section as a product of the ionization cross section $\sigma^{ion}(E)$ and a normalized energy distribution function. Rees *et al.* (1969) derived the energy distribution of the secondary electrons from the Bethe approximation and found

$$Q_{sec}(E, E_s) = \frac{1}{N} \frac{\exp[-0.0317(E_s + T) - 339 \exp(-0.402(E_s + T))]}{E_s + T} \times \ln \left[\frac{\sqrt{E} + \sqrt{E - E_s - T}}{\sqrt{E} - \sqrt{E - E_s - T}} \right], \quad (10)$$

where the energy of the incident electron is E , the energy of the secondary electron is E_s , the energy loss to the excited ion is T , and N is a normalization factor. Due to similar oscillator strengths of N_2 , O_2 , and O , Rees *et al.* (1969) find that Eq. (10) applies equally to these three species. Laboratory measurements were carried out by Opal *et al.* (1971, 1972) with N_2 and O_2 as target gases which gave similar energy distributions. Opal *et al.* (1971) fitted a function that is almost independent of the energy of the incident electron to their observations, i.e.

$$Q_{sec}(E, E_s) = \frac{1}{N} \frac{1}{1 + \left(\frac{E_s}{\bar{E}(E)} \right)^{2.1}}. \quad (11)$$

The parameter \bar{E} has only a weak dependence on the energy of the incident electron, E , and can be taken as a constant. For the three major neutral species in the thermosphere, the suggested values for \bar{E} are 13.0 eV, 17.4 eV, and 18.0 eV for N_2 , O_2 , and O respectively (Opal *et al.*, 1971; Strickland *et al.*, 1976). It should be noted that the measurements of Opal *et al.* (1971) extended to energies of the secondary electron to the smaller value of $\frac{1}{3}E$ or 200 eV. The fit of Eq. (11) represents these measurements with an accuracy of 20%. For secondary electron energies higher than 200 eV, we extrapolate Eq. (11). Figure 2 shows a comparison of the normalized secondary electron distribution resulting from incident electrons with 1 keV energy using Eq. (10) and Eq. (11). For this figure we used an energy loss to the neutrals of $T = 20$ eV and $\bar{E} = 13$ eV. Although the differences are small, we shall discuss the sensitivity of the result of the transport calculation to these differences in a later section.

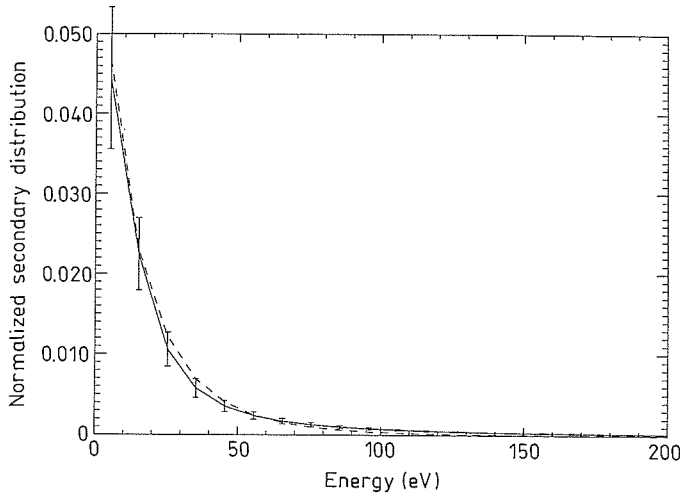


Fig. 2. Normalized energy distribution function for the secondary electron emerging from an ionization collision between a 1 keV electron and a nitrogen molecule. The solid line is from Opal *et al.* (1971) with $\bar{E} = 13.0$, the vertical bars indicate the 20% accuracy of Opal's parameterization. The dashed line is from Rees *et al.* (1969)

4 Comparison with experiment and other models

4.1 Laboratory experiments

In order to avoid the complexities of a simulation of a real auroral event, we will first compare the transport code to laboratory experiments on electron transport through neutral gas by Barrett and Hays (1976). In these experiments, an electron beam was made to penetrate into a chamber filled with rarefied neutral N_2 gas. The resulting emission of the $N_2^+ 1N$ bands was observed as a function of penetration depth. This experiment was carried out for electron beams at several energies. We have set up the transport code to simulate these experiments. Although injected as a beam into the collision chamber, the electrons in the laboratory were not confined by a magnetic field. Consequently the beam spreads out as soon as the electrons undergo collisions with the ambient gas. Auroral electrons on the other hand are confined by the geomagnetic field and angular scattering results in changes of pitch angle, but causes only very little spreading of the beam of incident electrons (Berger *et al.*, 1970). If the penetration into the collision chamber is measured by integrating the resulting luminosity in the chamber over slices perpendicular to the beam rather than radially from the nozzle of the electron gun, the obtained range of the electrons is equivalent to the auroral case.

We simulate the laboratory experiment by setting up an atmosphere of constant density, and inject an electron beam of intensity I_0 with a Gaussian energy distribution of mean energy E_0

$$I_0(E, \mu) = A(\mu)e^{-(E-E_0/E_h)^2}. \quad (12)$$

The halfwidth is chosen to be $E_h = 0.1E_0$, and the magnitude $A(\mu)$ is such that the spectrum carries an energy flux

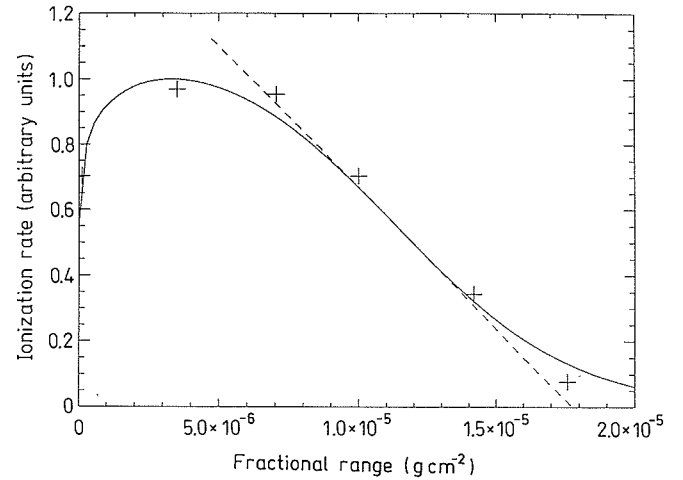


Fig. 3. Normalized ionization rate as a function of fractional range. The solid line is the result of the transport code, the crosses are from the Barrett and Hays (1976) experiment. The dashed line shows the tangent to the down-sloping part of the curve. The intersection of this tangent with the abscissa gives the range

F_E of $1 \text{ erg cm}^{-2} \text{ s}^{-1}$, where

$$F_E = 2\pi \int_{-1}^0 \mu d\mu \int_0^\infty I_0(E, \mu) E dE. \quad (13)$$

The initial angular distribution has little effect on the maximum penetration but determines the energy deposition profile along the path of penetration. Similarly, different spectral shapes have little influence on the calculated range but mostly determine the shape of the energy deposition function along the path of penetration. We have filled our simulation space with N_2 gas with a density high enough that no electrons reach the end of the box for a given length. To obtain results that are invariant to the density and dimensions of the box, we represent the penetration into the box in terms of the fractional range R in units of g cm^{-2}

$$R(z) = \int_0^z \rho(z') dz', \quad (14)$$

where ρ is the mass density of the gas and z is the distance into the box.

Figure 3 shows as an example the ionization rate calculated from the transport code as a function of fractional range. An incident spectrum with $E_0 = 2 \text{ keV}$ and a forward peaked angular distribution was input in both the experiment and the simulation. The plot shows only the first section of the entire length of the box which extended to $3 \times 10^{-5} \text{ g cm}^{-2}$. The energy flux reaching this depth is negligible. We have made similar calculations with mono-energetic and Maxwellian injection spectra. The tail end of the energy deposition or ionization rate as a function of fractional range (for this case the part of the graph above about $1.8 \times 10^{-5} \text{ g cm}^{-2}$) becomes more pronounced for Maxwellian spectra and less for mono-energetic spectra. Also shown are crosses to represent the measurements of the $N_2^+ 1N$ emission rate of Barrett and

Hays (1976) from their 2 keV experiment. Figure 7 of the Barrett and Hays (1976) paper is inconsistent with the text and tables in that paper (Paul Hays, personal communication, 1993), and for our comparison we rescaled the fractional range given in that figure to the range given in Table 1 of Barrett and Hays (1976) by a factor of 1.77/1.61. Since the measurements are given in units of counts per second, we normalized both graphs shown in Fig. 3 to the peak of the ionization rate. The range is defined by the intersection of a tangent at the nearly straight section of the energy deposition function and the abscissa. This tangent is indicated by the dashed line. The range in this case is $1.81 \times 10^{-5} \text{ g cm}^{-2}$, consistent with Barrett and Hays (1976) who measured a range of $1.77 \times 10^{-5} \text{ g cm}^{-2}$. We have made similar calculations with different angular distributions which gave a range between 1.70×10^{-5} and $1.81 \times 10^{-5} \text{ g cm}^{-2}$ depending on the non-isotropy of the boundary condition. The lowest value resulted from an isotropic boundary condition.

We repeated the range calculations for boundary conditions given by incident spectra covering the energy range from 300 eV to 8 keV. The shape of the ionization versus range curve is invariant to the initial energy of the incident electrons over this energy range, as was also found in experiments by Barrett and Hays (1976), Cohn and Caledonia (1970), and Grün (1957). Figure 4 shows the range from these calculations as a function of the mean energy of the incident beam. The experimental results of Barrett and Hays (1976) are shown by crosses. Cohn and Caledonia (1970) conducted a similar experiment with electron energies ranging from 2 to 5 keV and their results are shown by triangles. The dashed line gives an extrapolation of Grün's (1957) measurements which were made at 5 keV and above. The agreement of our model calculations with the experimental results remains unchanged for variations of the numerical energy grid or altitude grid as long as the number of grid points is not too small. The results of two model calculations are shown using either the secondary electron energy distribution function given by Opal *et al.* (1971) or by Rees *et al.* (1969). Cross section set 2 is used in both cases. Although the difference between these two secondary electron energy distribution functions is small, the range obtained from the Opal *et al.* (1971) formula for an 8 keV Gaussian input spectrum is about 20% smaller compared to the range obtained using the Rees *et al.* (1969) formula. Inspection of Fig. 2 reveals that the largest relative difference between the two formulas appears at high energies, above about 75 eV. This means that using Opal's formula, relatively more high-energy secondary electrons are produced in an ionization, and the incident electron loses relatively more energy than with Rees' formula. With cross sections decreasing with increasing energy above about 100 eV, the energetic incident beam experiences an ever increasing scattering depth as it degrades in energy. Thus the larger production of energetic secondary electrons and the resulting increased energy degradation causes an overall shorter range for the electrons.

We have also carried out calculations with the two different cross section sets and with different energy losses.

As discussed earlier, the energy loss in a collision is higher than the excitation threshold of the excited state, and we take this into account by assuming an energy loss 5% and 10% higher than the threshold energy. Comparing the calculated range using this energy loss rather than the excitation threshold shows that the 5% increase in energy loss results in approximately a 2% shorter range. Comparing the range when using the two different cross section sets shows that set 2 results in a 13% reduction relative to set 1. Using all combinations of cross section sets, energy losses, and secondary energy distribution functions as discussed above, the range for the 2 keV case ranges from $1.55 \times 10^{-5} \text{ g cm}^{-2}$ to $2.15 \times 10^{-5} \text{ g cm}^{-2}$, with the measured value from Barrett and Hays (1976) of $1.77 \times 10^{-5} \text{ g cm}^{-2}$. We obtain the best agreement between the measurements and the transport calculations using Opal's secondary electron distribution in combination with cross section set 1, or Rees' secondary electron distribution with cross section set 2. The results from all combinations of cross section sets and energy loss functions are summarized in Fig. 5. The figure demonstrates that the choice of cross section set has about as much influence on the range as the secondary energy

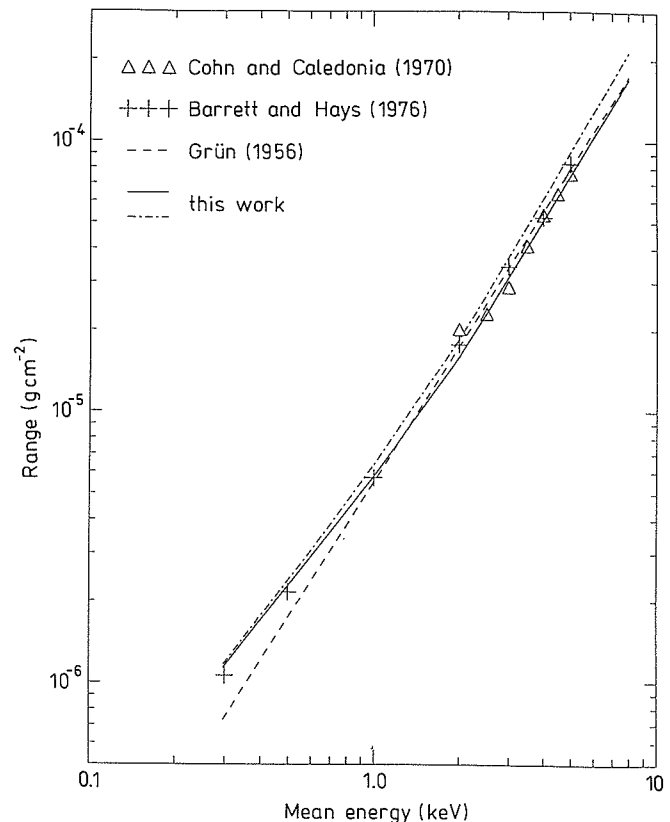


Fig. 4. Maximum range as a function of mean electron energy. The solid and dash-dot lines are from the transport calculation with strongly peaked narrow Gaussian input spectra. The solid line gives the range using the Opal *et al.* (1971) secondary electron distribution function, the dash-dot line results from the Rees *et al.* (1969) secondary distribution. Both calculations were made with cross section set 2. Also shown are measurements from Barrett and Hays (1976) and Cohn and Caledonia (1970), and an extrapolation from Grün's (1957) measurements

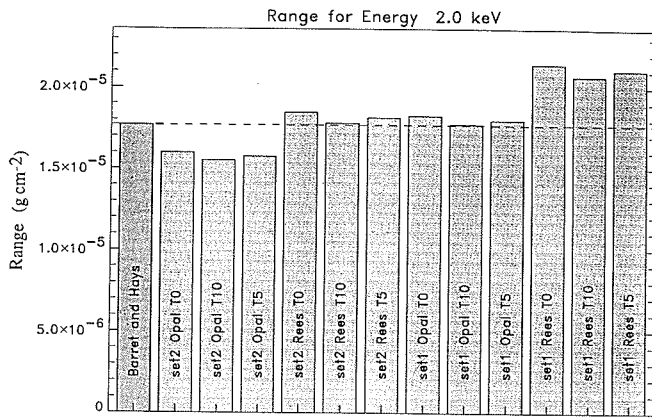


Fig. 5. Comparison between the range of 2 keV electrons calculated from the transport code and the Barrett and Hays (1976) measurements. The labels on the columns identify the cross sections set (set 1 or 2), the secondary energy distribution function [Opal *et al.* (1971), or Rees *et al.* (1969)], and the energy loss in excitation collisions (T0: energy loss equals the threshold energy; T5 and T10: energy loss is the threshold energy increased by 5% or 10%)

distribution functions have, but that the knowledge of the energy loss in excitation collisions is less critical.

The uncertainties in the Barrett and Hays (1976) measurements and uncertainties introduced into the transport calculation from other sources than the secondary electron energy distribution functions do not warrant using the differences in the graphs of Figs. 4 and 5 to determine a preferred function for the calculation of secondary electrons or cross section set. Rather, the conclusion that we can draw is that the range as determined by the transport calculation is accurate to only 20%, due to the uncertainties of the input parameters.

4.2 Energy conservation and comparison with other models

In the photoelectron case two aspects favour the numerical solution: the electron intensity in Eq. (1) is dominated by the photoelectron source term for altitudes below about 300 km (Link, 1992), and the energy range of interest is below about 1 keV (Winningham *et al.*, 1989), allowing a high resolution energy grid. This means that numerical problems from the scattering and penetration calculation may be masked by the source term, and the energy degradation calculation does not face the problem of large mismatches between the resolution of the numerical grid and the energy losses suffered by electrons. In the following we thus limit ourselves to the more difficult case – from the point of view of solving the transport equation numerically – namely the transport of auroral electrons.

The transport equation, Eq. (1), is solved for the electron intensity $I(z, E, \mu)$ as a function of altitude, energy, and pitch angle for specified input parameters, neutral density, electron density and temperature, and incident electron spectrum. With this intensity, the excitation and ionization rates of the atmospheric constituents can be computed. The energy $\mathcal{E}(z)$ that is deposited in the atmosphere by ionization and excitation of neutrals can be

found from

$$\mathcal{E}(z) = Q_e(z) + \sum_{j,i} 2\pi n_i(z) \int_{-1}^1 d\mu \int_{T_j}^{E_{max}} dE \sigma_i^j(E) T_j I(z, E, \mu). \quad (15)$$

The summation extends over all species i with density $n_i(z)$ and all states j with cross section $\sigma_i^j(E)$ and energy loss T_j ; $Q_e(z)$ is the energy deposited in the ambient electrons. The ambient thermal gas is heated through energy loss of the streaming electrons as described by the friction-like term containing the loss function $L(E)$ in Eq. (1) and through streaming electrons that are degrading into the thermal energy range. The heating rate is given by (Schunk and Nagy, 1978)

$$Q_e(z) = n_e \int_{E_t}^{\infty} L(E) \bar{I}(z, E) dE + n_e (E_t - \frac{3}{2} k T_e) (L(E_t) \bar{I}(z, E_t)). \quad (16)$$

The energy E_t is the energy where the intensities of the streaming electrons and the thermal electrons cross over i.e. the electron distribution is dominated by the thermal electrons below E_t and by the streaming electrons above E_t . T_e is the temperature of the ambient electrons with density n_e . The mean intensity $\bar{I}(z, E)$ is the integral of the intensity over solid angle. The loss function $L(E)$ in units of eV cm^2 is given by Swartz *et al.* (1971) in a parameterized analytic form

$$L(E) = \frac{3.37 \cdot 10^{-12}}{E^{0.94} n_e^{0.03}} \left(\frac{E - T_e}{E - 0.53 T_e} \right)^{2.36}. \quad (17)$$

The energy E and temperature T_e of the electrons are in units of eV in this parameterization. The loss function includes energy loss through Coulomb collision and Čerenkov wave generation.

The relative contribution to the heating of ambient electrons of the two terms in Eq. (16) depends mostly on the cross-over energy E_t . This in turn is controlled by the density and temperature of the ambient electron gas as well as by the intensity of the streaming electrons. For most auroral conditions the direct heating [first term in Eq. (16)] is the dominant term. The surface term [second term in Eq. (16)] contributes about 30% of the total heating at F-region altitudes. At E-region levels the ambient electrons are cooler than in the F-region, and the intensity of the auroral electrons in the energy range below 100 eV where the heating is most effective is largest. The surface term becomes less important at this altitude for intense aurora.

The total energy deposition rate in the atmosphere is given by the integral over altitude of $\mathcal{E}(z)$, and should equal the net energy flux through the upper boundary. The bottom boundary is selected such that the energy and particle flux through it are negligible. Thus we expect

$$\int_{z_0}^{z_M} \mathcal{E}(z) dz = 2\pi \int_0^{\infty} \int_{-1}^0 I(z_M, E, \mu) \mu d\mu E dE - 2\pi \int_0^{\infty} \int_0^1 I(z_M, E, \mu) \mu d\mu E dE. \quad (18)$$

Here, z_0 and z_M are the lower and upper boundary altitudes. For our numerical solution of the transport equation, this condition holds within 5% for energy grids extending to 70 keV which accommodate Maxwellian input spectra with characteristic energies up to $E_c = 10$ keV.

We have selected a moderately disturbed MSIS-90 (Hedin, 1991) winter atmosphere ($F_{10.7} = 150$, $A_p = 100$) which gave rise to an exospheric temperature of 1200 K, and the location of Poker Flat, Alaska, to simulate typical auroral conditions. The upper boundary condition was specified at 500 km altitude by isotropic Maxwellian input spectra with characteristic energies, E_c , from 100 eV to 10 keV. Aside from the energy conservation requirement Eq. (18), the energy loss per ion pair production gives an indication of possible numerical errors. For input spectra with $E_c = 300$ eV and above, the transport calculations yield an average energy loss per ion pair production between 35 and 37 eV, in good agreement with published data.

Figure 6 shows a detailed comparison between our computed electron fluxes with those obtained from Solomon (1993) in a Monte Carlo simulation. Using identical model atmospheres and incident electron spectra, we find good agreement between these two methods throughout the atmosphere and at all energies. The incident spectrum is defined by a Maxwellian energy distribution at 500 km altitude with a downward isotropic pitch angle distribution, a characteristic energy of $E_c = 1$ keV, and an energy flux of $1 \text{ erg cm}^{-2} \text{ s}^{-1}$. Also shown in Fig. 6 are the computed ionization rates of N_2^+ and O^+ as a function of altitude.

In order to compare our model results to other previously published auroral electron transport results, we determined the altitude where the N_2 ionization rate has

its maximum and show it as a function of characteristic energy in Fig. 7. This figure also shows the corresponding altitudes computed by Solomon (1993), Berger *et al.* (1970), and Strickland *et al.* (1989). Some scatter from the various methods is to be expected due to differences in the adopted cross sections and neutral densities, however, the agreement among the models is good. As was the case for the range calculations, using the secondary electron energy distribution function from Opal *et al.* (1971) leads to less penetration compared to using the formula from Rees *et al.* (1969). The differences are too small to have physical significance, but demonstrate that uncertainties in the input parameters to the transport calculation can account for variability in the altitude of the ionization rates of about half a scale height.

4.3 Comparison with auroral observations

Ground-based optical observations in the magnetic zenith can be compared with height-integrated emission rates computed with the auroral model. Emissions that are due to allowed transitions from states that are exclusively excited by electron impact are most suitable for such comparisons. Forbidden transitions have too many competing source and loss mechanisms to be a reliable indicator of possible problems in the solution of the transport equation. Even without knowledge of the incident electron spectrum responsible for the emissions it is possible to compare optical observations to the model. The transport equation is a linear integro-differential equation and thus the excitation rates are proportional to the incident energy flux. The altitude of an emission is controlled by

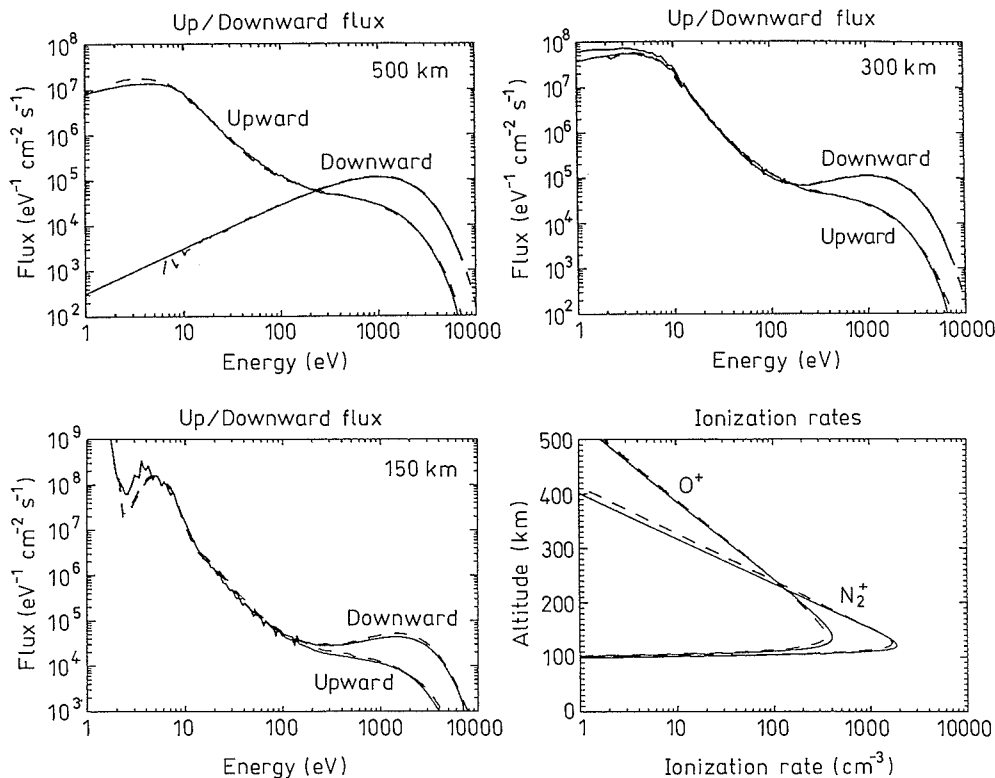


Fig. 6. Downward and upward electron fluxes as a function of energy for three altitudes (150, 300, 500 km) from a 1 keV Maxwellian incident spectrum. The solid lines are from this work, the dashed lines are from a Monte Carlo calculation by Solomon (1993). Also shown are the resulting N_2^+ and O^+ ionization rates as a function of altitude. The transport calculation used cross section set 1

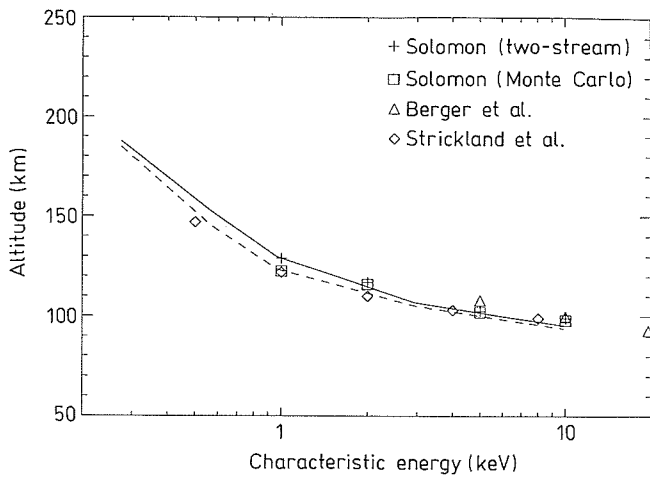


Fig. 7. The altitude of the maximum of the N_2 ionization rate as a function of characteristic energy of incident electron spectra. The *solid* and *dashed* lines show the altitudes from the present investigation, using the secondary electron distribution functions from Opal *et al.* (1971) and Rees *et al.* (1969) respectively. Cross section set 1 was used for both cases. The symbols represent previously published values from Solomon (1993), Berger *et al.* (1970), and Strickland *et al.* (1989)

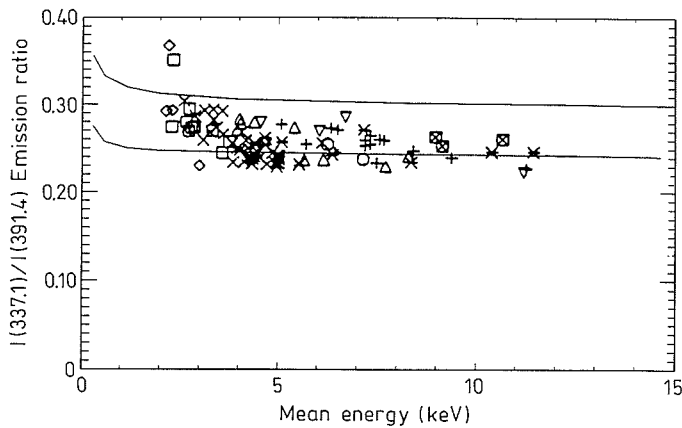


Fig. 8. Observations from Gattinger *et al.* (1991) of the $I(3371 \text{ \AA})/I(3914 \text{ \AA})$ emission ratio as a function of mean energy of the precipitating electrons. The *solid* lines show the largest and smallest ratio from our model, using cross section set 1 with the Opal *et al.* (1971) secondary electron distribution function, and cross section set 2 with the Rees *et al.* (1969) secondary electron distribution function

the combination of the characteristic energy and the neutral density distribution in the atmosphere. Selecting auroral spectral features that are not subject to absorption in the atmosphere, the surface brightness at the ground can be related to the height-integrated emission without knowledge of the altitude distribution.

Although the absorption of the $N_2^+1N(4278 \text{ \AA})$ band is substantial in the atmosphere, most of the absorption occurs in the troposphere, and uncertainties in the height of the aurora do not contribute to uncertainties in the height-integrated emission rate. Observations from the ground as well as optical observations from a satellite have shown that the height-integrated emission rate of $N_2^+1N(4278 \text{ \AA})$ is nearly independent of the characteristic

energy and shape of the incident electron spectrum, at about $250 \text{ R}(\text{erg cm}^{-2} \text{ s}^{-1})^{-1}$. The model calculations also yield this constant emission rate. The brightness of the N_2^+1N band is thus useful as a normalization parameter for other optical emissions. In particular, the ratio of the surface brightness of the N_22P to N_2^+1N bands has been investigated in detail after Rees and Lummerzheim (1989) suggested a variation of this ratio with the characteristic energy of the incident spectrum. Model calculations by Richards and Torr (1990), Strickland *et al.* (1989), and Solomon (1993) all show that this ratio should be independent of the characteristic energy. Observations by Gattinger *et al.* (1991) confirm these model predictions. The prediction of Rees and Lummerzheim (1989) was based on the transport calculations by Lummerzheim (1987). The disagreement of the prediction with the observations indicates an inaccurate solution to the transport calculation. The excitation cross section for the $N_2(C^3\Pi)$ state from which the N_22P emission originates peaks at low energies where the electron intensity is dominated by secondary electrons from ionization collisions. We have changed the numerical implementation of the source for secondary electrons and have updated the cross sections used in the transport calculation. The new code results in a $N_22P(3371 \text{ \AA})$ to $N_2^+1N(4278 \text{ \AA})$ emission ratio that is in agreement with the measurements of Gattinger *et al.* (1991). Figure 8 is a reproduction from Gattinger *et al.* (1991) with our model results superimposed. Their observations of the $N_22P(3371 \text{ \AA})$ to $N_2^+1N(3914 \text{ \AA})$ ratio gave a constant value of 0.3 with less than 15% variation over the energy range from 2 to 12 keV. This ratio is equivalent to a ratio of $I(3371 \text{ \AA})/I(4278 \text{ \AA}) = 0.99$, using the Franck-Condon factors from Vallance Jones (1974). For our auroral calculation we find nearly constant values for the emission ratio from incident electron spectra with characteristic energies from a fraction of a keV to several keV. Depending on the cross section set and secondary electron energy distribution function, this ratio takes a value between 0.85 and 1.0 [cross section set 1 with the Opal *et al.* (1971) secondary distribution leads to the highest ratio, cross section set 2 with the Rees *et al.* (1969) secondary distribution gives the lowest value; the N_22P emission cross section in both sets have the same peak value and are in agreement with Cartwright *et al.* (1977)]. Other published values derived from model calculations are 0.98 from Richards and Torr (1990) and 0.9 from Solomon (1993). Gattinger *et al.* (1991) note that the absolute value of their observed ratio might be in error by 15% due to instrumental uncertainties. The model value is based on emission cross section measurements which induce a 20% uncertainty (Cartwright *et al.*, 1977) of the N_22P emission in addition to numerical uncertainties. Within these errors, the observations and model results are in agreement not only concerning the constancy of the ratio, but also with respect to the magnitude of the ratio.

5 Conclusion

We have presented here an electron transport calculation that forms the heart of an auroral model. This new numerical

model corrects errors of a previously published transport code. We have tested and analysed the performance of the new transport code, and compared its results to problems with analytic solutions, laboratory measurements, and auroral observations. With our numerical model we can reproduce the laboratory observations of electron penetration into N_2 gas by Barrett and Hays (1976), and auroral emission ratio measurements by Gattinger *et al.* (1991).

The uncertainty of the calculated ionospheric and auroral parameters depends mostly on uncertainties in the available input parameters. An internal check of energy conservation (Eq. 18) on the numerical grid suggests that the numerical procedure introduces an error of less than 5% to the results. Cross section measurements have large uncertainties and the total loss cross section has an uncertainty of 20% or more. We have investigated the sensitivity of the model results to such uncertainties in the cross sections by comparing results that were obtained using two different sets of cross sections. The double differential cross sections that describe the energy and angle distribution of secondary electrons emerging from ionization collisions are most important to know. Although the angular distribution of secondary electrons has little influence on the angular distribution of the low energy electron intensity, the energy distribution of the secondary electrons has to be known with some accuracy. A widely used parameterization by Opal *et al.* (1971) has an uncertainty of 20% and agrees with a theoretically derived secondary electron energy distribution function by Rees *et al.* (1969) within this uncertainty. For range calculations, the difference between these two formulas for the secondary energy distribution can result in differences of 20% in range. Applied to auroral calculations, we find differences in the altitude of the maximum of the ionization rate of up to half a scale height.

We find that the ratio of the $N_2 2P(3371 \text{ \AA})$ to the $N_2^+ 1N(4278 \text{ \AA})$ emission is independent of the incident electron spectrum but varies between values of 0.85 and 1.0 when we use combinations of different cross section sets and secondary electron energy distribution functions. The column integrated emission rate of $N_2^+ 1N(4278 \text{ \AA})$ takes values between 220 and 270 R for a 2 keV Maxwellian incident electron intensity with an energy flux of $1 \text{ erg cm}^{-2} \text{ s}^{-1}$, using identical emission cross sections, but different energy loss cross sections and secondary electron energy distribution functions. Based on the numerical experiments presented here, we conclude that the uncertainty of integrated electron fluxes from electron transport calculations in the aurora is no less than 15–20%. For auroral modeling this uncertainty is increased by uncertainties due to lack of accurate knowledge of atmospheric densities and particle precipitation. Calculated individual emissions have an additional error associated with the emission cross section itself.

Acknowledgements. The authors would like to thank M. H. Rees for many valuable discussions and suggestions. We thank S. C. Solomon, who made results from his Monte Carlo simulation available to us, and E. S. Oran for providing cross sections. This work was partially funded by the University of Alaska through NSF grant

ATM90-22197 and NASA grant NAGW-3037. This work has been partly supported by the GRECO PLASMAE of CNRS of France.

The Editor-in-Chief would like to thank three referees for their help in evaluating this paper.

References

- Ajello, J. M., and D. E. Shemansky, A re-examination of important N_2 cross sections by electron impact with application to the dayglow: the Lyman-Birge-Hopfield band system and NI (119.99 nm), *J. Geophys. Res.*, **90**, 9845, 1985.
- Banks, P. M., and A. F. Nagy, Concerning the influence of elastic scattering upon photoelectron transport and escape, *J. Geophys. Res.*, **75**, 1902, 1970.
- Banks, P. M., C. R. Chappell, and A. F. Nagy, A new model for the interaction of auroral electrons with the atmosphere: spectral degradation, backscatter, optical emission, and ionization, *J. Geophys. Res.*, **79**, 1459, 1974.
- Barrett, J. L., and P. B. Hays, Spatial distribution of energy deposited in nitrogen by electrons, *J. Chem. Phys.*, **64**, 743, 1976.
- Berger, M. J., S. M. Seltzer, and K. Maeda, Energy deposition by auroral electrons in the atmosphere, *J. Atmos. Terr. Phys.*, **32**, 1015, 1970.
- Borst, W. L., and E. C. Zipf, Cross section for electron impact excitation of the (0, 0) first negative band and N_2^+ from threshold to 3 keV, *Phys. Rev. A*, **1**, 834, 1970.
- Cartwright, D. C., S. Trajmar, A. Chutjian, and W. Williams, Electron impact excitation of the electronic states of N_2 . II. Integral cross sections at incident energies from 10 to 50 eV, *Phys. Rev. A*, **16**, 1041, 1977.
- Christensen, A. B., L. R. Lyons, J. H. Hecht, G. G. Sivjee, R. R. Meier, and D. G. Strickland, Magnetic field-aligned electric field acceleration and the characteristics of the optical aurora, *J. Geophys. Res.*, **92**, 6163, 1987.
- Cicerone, R. J., W. E. Swartz, R. S. Stolarski, A. F. Nagy, and J. S. Nisbet, Thermalization and transport of photoelectrons: a comparison of theoretical approaches, *J. Geophys. Res.*, **78**, 6709, 1973.
- Cohn, A., and G. Caledonia, Spatial distribution of the fluorescent radiation emission caused by an electron beam, *J. Appl. Phys.*, **41**, 3767, 1970.
- Gattinger, R. L., A. Vallance Jones, J. H. Hecht, D. J. Strickland, and J. Kelly, Comparison of ground-based optical observations of N_2 second positive to N_2^+ first negative emission ratios with energy precipitation energies inferred from the Sondre Stromfjord radar, *J. Geophys. Res.*, **96**, 11,341, 1991.
- Germany, G. A., M. R. Torr, P. G. Richards, and D. G. Torr, The dependence of modeled OI 1356 and N_2 Lyman-Birge-Hopfield auroral emissions on the neutral atmosphere, *J. Geophys. Res.*, **95**, 7725, 1990.
- Green, A. E. S., and R. S. Stolarski, Analytic models of electron impact excitation cross sections, *J. Atmos. Terr. Phys.*, **34**, 1703, 1972.
- Grün, A. E., Lumineszenz-photometrische Messungen der Energieabsorption im Strahlungsfeld von Elektronenquellen: Eindimensionaler Fall in Luft, *Z. Naturforsch.*, **12**, 89, 1957.
- Hedin, A. E., Extension of the MSIS thermosphere model into the middle and lower atmosphere, *J. Geophys. Res.*, **96**, 1159, 1991.
- Ishimoto, M., C.-I. Meng, G. J. Romick, and R. E. Huffman, Auroral energy electron flux from molecular nitrogen ultraviolet emissions observed by S3-4 satellite, *J. Geophys. Res.*, **93**, 9854, 1988.
- Jackman, C. H., R. M. Garvey, and A. E. S. Green, Electron impact on atmospheric gases, I. Updated cross sections, *J. Geophys. Res.*, **82**, 5081, 1977.
- Jasperse, J. R., Boltzmann-Fokker-Planck model for the electron distribution function in the Earth's atmosphere, *Planet. Space Sci.*, **24**, 33, 1976.
- Jasperse, J. R., and D. J. Strickland, Approximate analytic solutions for the primary auroral electron flux and related quantities, AFGL-TR-81-0069, Air Force Geophysics Laboratory, 1981.

- Kasting, J. F., and P. B. Hays**, A comparison between N_2^+ 4278 Å emission and electron flux in the auroral zone, *J. Geophys. Res.*, **82**, 3319, 1977.
- Lie-Svendsen, Ø, M. H. Rees, and K. Stamnes**, Helium escape from the Earth's atmosphere: the charge exchange mechanism revisited, *Planet. Space Sci.*, **40**, 1639, 1992.
- Liliensten, J., D. Fontaine, W. Kofman, L. Eliasson, C. Lathuillere, and E. S. Oran**, Electron energy budget in the high-latitude ionosphere during VIKING/EISCAT coordinated measurements, *J. Geophys. Res.*, **95**, 6081, 1990.
- Link, R.**, Dayside magnetospheric cleft auroral processes, Ph.D. Thesis, York University, Toronto, Canada, 1982.
- Link, R.**, Feautrier solution of the electron transport equation, *J. Geophys. Res.*, **97**, 159, 1992.
- Link, R., S. Chakrabarti, G. R. Gladstone, and J. C. McConnell**, An analysis of satellite observations of the OI EUV dayglow, *J. Geophys. Res.*, **93**, 14,631, 1988.
- Lummerzheim, D.**, Electron transport and optical emissions in the aurora, Ph.D. Thesis, University of Alaska, Fairbanks, 1987.
- Lummerzheim, D., M. H. Rees, and H. R. Anderson**, Angular dependent transport of auroral electrons in the upper atmosphere, *Planet. Space Sci.*, **37**, 109, 1989.
- Lummerzheim, D., M. H. Rees, and G. J. Romick**, The application of spectroscopic studies of the aurora to thermospheric neutral composition, *Planet. Space Sci.*, **38**, 67, 1990.
- Lummerzheim, D., M. H. Rees, J. D. Craven, and L. A. Frank**, Ionospheric conductances derived from DE-1 auroral images, *J. Atmos. Terr. Phys.*, **53**, 281, 1991.
- Mantas, G. P.**, Theory of photoelectron thermalization and transport in the ionosphere, *Planet. Space Sci.*, **23**, 337, 1974.
- Min, Q. L., D. Lummerzheim, M. H. Rees, and K. Stamnes**, The effects of a parallel electric field and the geomagnetic field in the topside ionosphere on auroral and photoelectron energy distributions, *J. Geophys. Res.*, **98**, 19,223, 1993.
- Nagy, A. F., and P. M. Banks**, Photoelectron fluxes in the ionosphere, *J. Geophys. Res.*, **75**, 6260, 1970.
- Opal, C. B., W. K. Peterson, and E. C. Beaty**, Measurements of secondary-electron spectra produced by electron impact ionization of a number of simple gases, *J. Chem. Phys.*, **55**, 4100, 1971.
- Opal, C. B., E. C. Beaty, and W. K. Peterson**, Tables of secondary electron-production cross sections, *Atomic Data*, **4**, 209, 1972.
- Oran, E. S., and D. J. Strickland**, Photoelectron flux in the Earth's ionosphere, *Planet. Space Sci.*, **26**, 1161, 1978.
- Porter, H. S., and F. W. Jump, Jr.**, Analytic total and angular elastic electron impact cross sections for planetary atmospheres, *Tech. Rep. CSC/TM-6017*, Goddard Space Flight Center, Greenbelt, Md., 1978.
- Porter, H. S., F. Varosi, and H. G. Mayr**, Iterative solution of the multistream transport equation. 1. Comparison with laboratory beam injection experiments, *J. Geophys. Res.*, **92**, 5933, 1987.
- Pritchford, L. C., and A. V. Phelps**, Comparative calculations of electron-swarm properties in N_2 at moderate E/N values, *Phys. Rev. A*, **25**, 540, 1982.
- Rapp, D., and P. Englander-Golden**, Total cross sections for ionization and attachment in gases by electron impact. I. Positive ionization, *J. Chem. Phys.*, **43**, 1464, 1965.
- Rees, M. H.**, Auroral ionization and excitation by incident energetic electrons, *Planet. Space Sci.*, **11**, 1209, 1963.
- Rees, M. H., and D. Luckey**, Auroral electron energy derived from ratio of spectroscopic emissions. 1. Model computations, *J. Geophys. Res.*, **79**, 5181, 1974.
- Rees, M. H., and D. Lummerzheim**, Characteristics of auroral electron precipitation derived from optical spectroscopy, *J. Geophys. Res.*, **94**, 6799, 1989.
- Rees, M. H., A. I. Stewart, and J. C. G. Walker**, Secondary electrons in aurora, *Planet. Space Sci.*, **17**, 1997, 1969.
- Rees, M. H., D. Lummerzheim, R. G. Roble, J. D. Winningham, J. D. Craven, and L. A. Frank**, Auroral energy deposition rate, characteristic electron energy and ionospheric parameters derived from Dynamics Explorer 1 images, *J. Geophys. Res.*, **93**, 12,841, 1988.
- Richards, P. G., and D. G. Torr**, The altitude variation of the ionospheric photoelectron flux: a comparison of theory and measurement, *J. Geophys. Res.*, **90**, 2877, 1985.
- Richards, P. G., and D. G. Torr**, Auroral modeling of the 3371 Å emission rate: dependence on characteristic electron energy, *J. Geophys. Res.*, **95**, 10,337, 1990.
- Schunk, R., and A. F. Nagy**, Electron temperatures in the F-region of the ionosphere: theory and observations, *Rev. Geophys. Space Phys.*, **16**, 355, 1978.
- Solomon, S. C.**, Auroral transport using the Monte Carlo method, *Geophys. Res. Lett.*, **20**, 185, 1993.
- Stamnes, K.**, Analytic approach to auroral electron transport and energy degradation, *Planet. Space Sci.*, **28**, 427, 1980.
- Stamnes, K.**, On the two-stream approach to electron transport and thermalization, *J. Geophys. Res.*, **86**, 2405, 1981.
- Stamnes, K.**, The theory of multiple scattering of radiation in plane parallel atmospheres, *Rev. Geophys.*, **24**, 299, 1986.
- Stamnes, K., and M. H. Rees**, Inelastic scattering effects on photoelectron spectra and ionospheric electron temperature, *J. Geophys. Res.*, **88**, 6301, 1983.
- Stamnes, K., and P. Conklin**, A new multi-layer discrete ordinate approach to radiative transfer in vertically inhomogeneous atmospheres, *J. Quant. Spectrosc. Radiat. Transfer*, **31**, 273, 1984.
- Stamnes, K., S. C. Tsay, W. J. Wiscombe, and K. Jayaweera**, Numerically stable algorithm for discrete-ordinate-method radiative transfer in multiple scattering and emitting layered media, *Appl. Optics*, **27**, 2502, 1988.
- Stamnes, K., Ø. Lie-Svendsen, and M. H. Rees**, The linear Boltzmann equation in slab geometry: development and verification of a reliable and efficient solution, *Planet. Space Sci.*, **10**, 1435, 1991.
- Strickland, D. J., D. L. Book, T. P. Coffey, and J. A. Fedder**, Transport equation techniques for the deposition of auroral electrons, *J. Geophys. Res.*, **81**, 2755, 1976.
- Strickland, D. J., J. R. Jasperse, and J. A. Whalen**, Dependence of auroral FUV emissions on the incident electron spectrum and neutral atmosphere, *J. Geophys. Res.*, **88**, 8051, 1983.
- Strickland, D. J., R. R. Meier, J. H. Hecht, and A. B. Christensen**, Deducing composition and incident electron spectra from ground based auroral optical measurements: theory and model results, *J. Geophys. Res.*, **94**, 13,527, 1989.
- Swartz, W. E.**, Optimization of energetic electron energy degradation calculations, *J. Geophys. Res.*, **90**, 6587, 1985.
- Swartz, W. E., J. S. Nisbet, and A. E. S. Green**, Analytic expression for the energy-transfer rate from photoelectrons to thermal-electrons, *J. Geophys. Res.*, **76**, 8425, 1971.
- Vallance Jones, A.**, *Aurora*, Reidel, Dordrecht, 1974.
- Vallance Jones, A., R. L. Gattinger, P. Shih, J. W. Meriwether, V. B. Wickwar, and J. Kelly**, Optical and radar characterizations of a short-lived auroral event at high latitude, *J. Geophys. Res.*, **92**, 4575, 1987.
- Wadzinski, H. T., and J. R. Jasperse**, Low energy electron and photon cross sections for O, N_2 , and O_2 , and related data, AFGL-TR-82-0008, Air Force Geophysics Laboratory, 1982.
- Winningham, J. D., D. T. Decker, J. U. Kozyra, J. R. Jasperse, and A. F. Nagy**, Energetic (> 60 eV) atmospheric photoelectrons, *J. Geophys. Res.*, **94**, 15,335, 1989.
- Wiscombe, W. J.**, The delta-M method: rapid yet accurate radiative flux calculations for strongly asymmetric phase functions, *J. Atmos. Sci.*, **34**, 1408, 1977.

